Supporting Information

Multivariate biophysical markers predictive of mesenchymal stromal cell multipotency
Lee, Shi et al.

A. Supporting Text, Method Notes, Figures S1-8, Tables S1-4 & Discussion
B. Detailed Methods, including Supporting Figures S9-13
C. References

A. Supporting Text, Method Background and Notes, & Discussion

1. Previous studies noting one or more biophysical properties potentially indicative of stem cell phenotype

To understand our results that identified three specific biophysical markers predictive of multipotent MSC subpopulations in context, we here briefly discuss previous observations of heterogeneity in five biophysical properties of bone marrow-derived MSCs or other stem cells. These five characteristics include: (1) suspended-cell diameter; (2) adherent-cell spread area; (3) cell stiffness; (4) nuclear to cytoplasmic ratio (*N:C*); and (5) relative nuclear membrane fluctuations. *Cell size* differences among aMSCs were noted by Colter et al., who observed that smaller and spindle-like cells adherent to culture plastic maintained multipotency and proliferated more rapidly than larger cells within the aMSC population (1). MSCs derived from fetal bone marrow (fMSCs) are also uniformly smaller and proliferate more rapidly than heterogeneous aMSC cultures, and are trilineage multipotent (2, 3). Separate studies have shown that cell *size and viscoelastic properties* can correlate with differentiation fate of adipose-derived stem cells (4). Similarly, the pluripotency of human embryonic stem cells (ESCs) has been associated with lower cell *stiffness and higher nuclear membrane fluctuations*, which are thus proposed as relative signatures of undifferentiated stem cells (5, 6). Other potential biophysical markers of ESC pluripotency include a high *ratio of nucleus-to-cytoplasm* and a low *adherent cell spread area*; these have also been shown to individually correlate with stem cell differentiation capacity (5, 7). Thus, previous studies have considered one or, at most, two different biophysical characteristics that may relate to, variously, the multipotency or the pluripotency or the differentiation potential along a specific tissue lineage. These previous studies were also chiefly focused on *in vitro* rather than *in vivo* correlations and outcomes. Our present multivariate anlaysis described in the text enabled us to consider whether any, some sufficient set, or none of these biophysical characteristics can reliably predict an *in vitro* or *in vivo* indication of multipotency (or bipotency) in adult bone marrow-derived, culture expanded MSCs.

2. Method Background and Notes.

(a) Size-based cell sorting methods

Briefly, this microfluidic device separates particles under modest shear flow via competing inertial and Dean's drag forces, such that larger particles tend to sequester toward the channel wall. This flow-based device was employed because of its ease of use, high throughput function (3 x 10^6 cells/h), and high viability of sorted cells (>90% of the cells remained viable as assessed with Trypan Blue staining and the cells ability to attach when seeded), which enables large populations of MSCs to be assayed and subsequently analyzed. Subsequent to trypsinization, cells were collected at the outlets of the spiral microfluidic device as fractions or subpopulations of decreasing mean cell diameter (Outlet 1, 2, 3, and 4 respectively). Analyses of the collected adult MSCs (aMSCs) subpopulations from each of five donors (aD1-aD5) revealed that they were indeed heterogeneous in size, in both the suspended and adherent states (Fig. S1a-b). The spiral intertial microfluidic device allowed separation of aMSC subpopulations on the basis of suspended-cell diameter; Fig. S1c illustrates this for donor aD1, contrasting the diameter distributions of the unsorted aD1 MSCs at passage 5 with the sorted D^{hi} (Outlet 1) and D^{lo} (Outlet 4) subpopulations and the fD1 cells. D^{hi} and D^{lo} aMSCs also exhibited distinct adherent morphology: D^{hi} cells (Outlet 1) were more spread and enlarged while the D^{lo} cells (Outlet 4) were more spindle-like (Fig. S1d), consistent with previous reports by Colter et al.(1) In contrast, fMSCs were more homogenous in size and mostly spindle-shaped when adhered to tissue culture polystyrene (or glass).

As discussed in the text, D^{hi} subpopulations were consistently restricted in potency along osteochondral lineages *in vitro* (Table 1). Table S1 shows these data for adult and fetal at both passages 5 and 8. Also as discussed in the text, D^{hi} subpopulations contributed to more efficient bone remodeling in ectopic bone assays *in vivo* (Fig. 5). Such spiral, inertial microfluidic sorting thus enables efficient isolation of viable osteochondral progenitors from human bone marrow, for both *in vitro* and *in vivo* use.

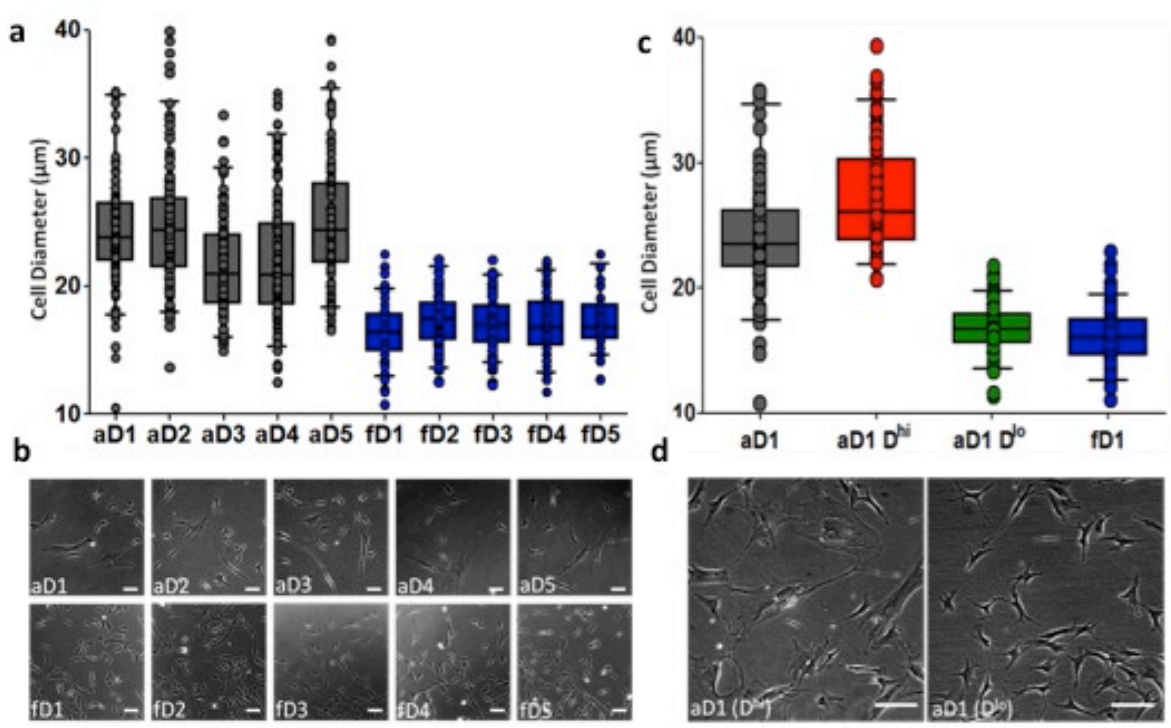

Figure S1. Cell size heterogeneity of culture-expanded mesenchymal stem cells. (a) Diameter of suspended cells and (b) morphology of adhered cells from adult donors (aD1-5) and fetal donors (fD1-5) at passage 5. (c) aMSCs are heterogeneous in diameter and were size sorted using a spiral microfluidic channel into Outlet 1 (D^{hi}) and Outlet 4 (D^{lo}) subpopulations for subsequent analysis. This example shows the unsorted (gray) and sorted (red and green) for aD1, in comparison to fD1; see Fig. S7 for all MSC donor sources. (d) After sorting, D^{hi} and D^{lo} aMSC subpopulations from aD1 exhibited distinct morphology when adhered to tissue culture polystyrene (or glass), as observed across all adult donors. Scale bars = 100 μm.

(b) Spectrophotometic quantification for MSC differentiation

Figure S2 quantifies spectroscopic measurements of differentiation, in terms of relative amounts of products indicative of differentiation along several lineages: adipogenic (Oil Red O), osteogenic (Alizarin Red S), chondrogenic (Alcian blue), and myogenic (desmin immunostaining). For each MSC donor (adult, aD1-5 and fetal fD1-5), we exposed the unsorted MSC population and the size-sorted D^{hi} and D^{lo} subpopulations to the appropriate induction medium under standard cell densities and induction protocols described in Methods. As an objective means to identify groups that had differentiated or not, the threshold level indicating positive or negative differentiation is shown in each graph. Here, the solid line indicated by the arrow represents the 90th percentile of the control condition, which were those MSCs cultured in non-induction medium (-ind). Positive differentiation was noted for subpopulations that showed phenotype-specific metabolite production or desmin-positive cells above the 90th percentile of corresponding controls. Notably, subpopulations from the same donor exhibited different amounts of metabolite (i.e., extent of differentiation) for

osteogenesis, even when comparing subpopulations that both differentiated (e.g., D^{hi} and D^{lo} subpopulations from aD1 to aD3).

Screening for Oil Red O optical densities revealed that the D^{lo} aMSCs were more adipogenic than the D^{hi} aMSCs (Fig. S2a). Similarly, immunostaining of desmin two weeks after the initial myogenic induction with 5'-azacytidine showed that the D^{lo} aMSCs subpopulations have a greater number of desmin positive cells (Fig. S2d). These results indicate a stronger myogenic potential in D^{lo} aMSCs. Conversely, Alizarin Red S optical densities for the D^{hi} aMSCs were significantly greater than those of the D^{lo} adult MSC subpopulations (Fig. S2b). For chondrogenic differentiation, there was no detectable difference in the extent of differentiation among the adult D^{hi}, D^{lo} and fetal MSCs (Fig. S2c).

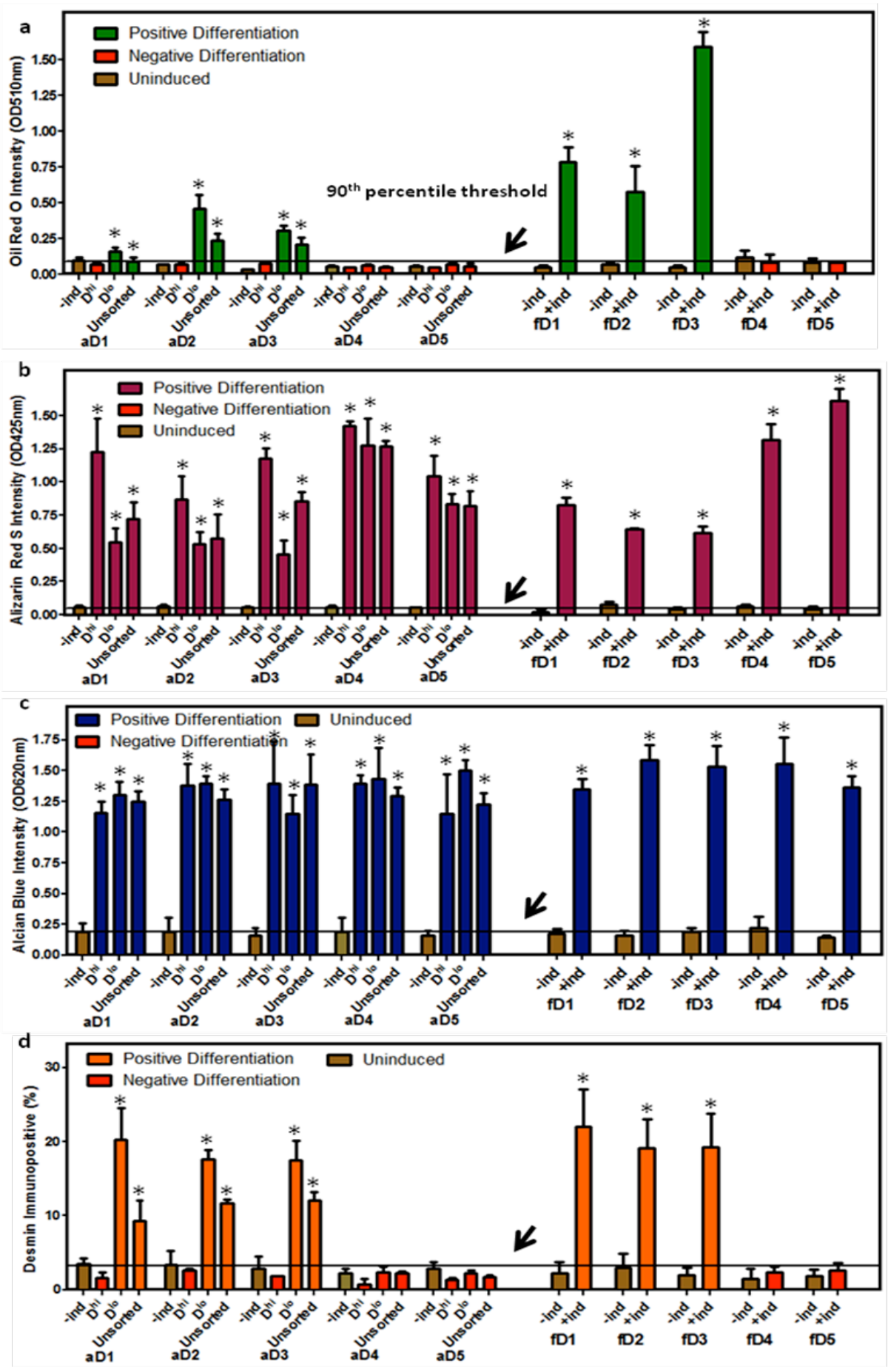
a
Positive Differentiation
Negative Differentiation
Uninduced
Oil Red O Intensity (OD510nm)
90th percentile threshold
b
Positive Differentiation
Negative Differentiation
Uninduced
Alizarin Red S Intensity (OD425nm)
c
Positive Differentiation
Negative Differentiation
Uninduced
Alcian Blue Intensity (OD620nm)
d
Positive Differentiation
Negative Differentiation
Uninduced
Desmin Immunopositive (%)
-ind
Dhi
Dlo
Unsorted
+ind
aD1
aD2
aD3
aD4
aD5
fD1
fD2
fD3
fD4
fD5

Figure S2. Spectrophotometric quantification of the amounts of lineage-specific metabolites produced by the different subpopulations of MSCs for (a) adipogenesis, (b) osteogenesis, (c) chondrogenesis. (d) As an indicator consistent with myogenesis, the number of desmin-positive cells were expressed as a percentage of the total number of cells counted (n = 164-420). Data are presented as arithmetic means ± SD. Asterisk denotes statistical significance at $\alpha = 0.05$ from corresponding controls (non-inductive media).

Figures S3-S4 show representative images from *in vitro* differentiation assays conducted for adult MSC D^{hi} and D^{lo} and for fetal MSCs, respectively. These images are a subset of those used to quantify differentiation via spectroscopy, as indicated in Fig. S2. Thus, in these images, differentiation is indicated by superthreshold positivity for Oil Red O (adipogenesis); Alizarin Red S (osteogenesis); Alcian blue (chondrogenesis); and desmin+ immunostaining (myogenesis).

While the D^{hi} MSC subpopulations from the different adult donors were consistently limited by differentiation toward the adipogenic (Fig. S3a) and myogenic (Fig. S3d) lineages, the D^{lo} MSC subpopulations were inconsistent in capacity for differentiation along additional lineages. Note that desmin expression is consistent with myogenic differentiation but is not a conclusive marker. *In vivo* assays of myogenic-like repair by these MSCs were further presented in Figure 5. While the D^{lo} MSCs from donors 1-3 (aD1-3) were multilineage, the D^{lo} MSCs from donors 3 and 4 (aD3 and 4) showed limited differentiation towards the adipogenic and myogenic lineage. No discernible differences could be observed in chondrogenesis among different subpopulations of adult MSCs.

MSCs from fetal donors showed variable extent of differentiation (Fig. S4), despite relatively homogeneous uniformity in suspended-cell diameter and attached-cell morphology as summarized in Fig. S1. Donor populations fD1-3 exhibited extensive differentiation along all four lineages, while fD4 and fD5 showed limited adipogenic and myogenic differentiation.

Thus, as discussed in the text, cell size alone is an insufficiently specific biophysical marker of MSC multipotency *in vitro*.

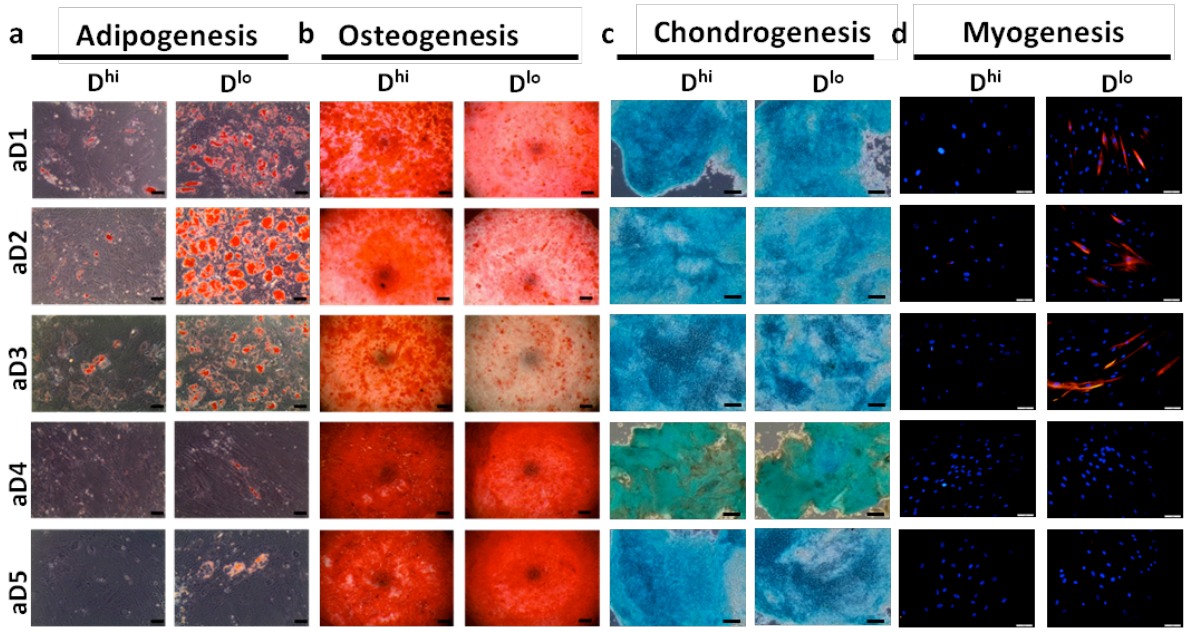

Figure S3. Cell size does not correlate consistently with heterogeneity in the differentiation behavior of MSCs among different adult donors into (a) adipogenic (b) osteogenic (c) chondrogenic and (d) myogenic lineages. Scale bar (a-c) = 250 μm; scale bar (d) = 50 μm.

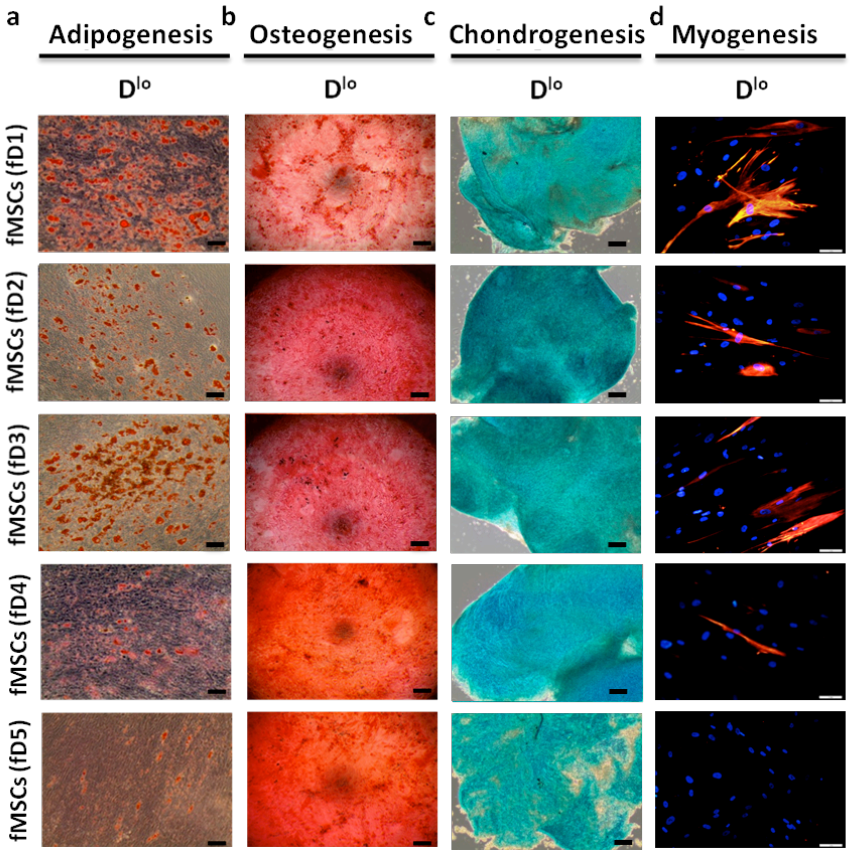

Figure S4. fMSCs showed variable extent of differentiation, despite relative homogeneous uniformity in suspended-cell diameter and attached-cell morphology. Donor populations fD1-3 exhibited extensive differentiation along all four lineages, while fD4 and fD5 showed limited adipogenic and myogenic differentiation. Scale bar (a-c) = 250 μm; scale bar (d) = 50 μm.

3. Microfluidic size-based sorting of MSCs does not alter *D*, *E*, or *NF*.

Spiral inertial microfluidic sorting does not change the three biophysical properties of MSCs associated with multipotency. **Figure S5** demonstrates this for donor aD3 as a representative example. These data are presented as probability distributions of measured *D*, *E* and *NF* for at least 30 cells per subpopulation for each property. The key point here is that the distributions of these biophysical properties are quite similar, whether or not cells have been physically sorted by size in this microfluidic device; inset data quantify *E* and *NF* in terms of mean +/- SEM.

Figure S5a compares the distribution of cell diameter *D* after passage of cells through the microfluidic device (post-sorting) vs. that for the population at the same passage that never passed through this device (unsorted). Cell diameter distribution of the overall population did not differ detectably upon sorting. Here, the graph shows the distribution of cell diameter for unsorted cells (those not passed through the device), as compared to Outlet 1 and Outlet 4, and then also compared to pooling the cell diameters from Outlets 1, 2, 3, and 4 (i.e., all the cells). The pooled "post-sorted" data is the solid black line in Fig. S5a, showing that the total population distribution of sizes well matches the distribution for cells from the same donor source and passage that were not exposed to the processing conditions and shear flows through the device.

Figure S5b shows that the distribution of mechanical stiffness distribution for cells sorted to Outlet 1 (O1, D^{hi}) and Outlet 4 (O4, D^{lo}) cells are consistent with the mechanical stiffness of unsorted large cells (cell spread area > 5500 um^2) and small cells (spread area < 5000 um^2). These distributions represent *E* for the size-sorted subpopulations in Outlet 1 and Outlet 4, as compared to the largest and smallest cells, respectively in an unsorted population. Here, note that the cells are attached in both the unsorted and sorted cases. We have already confirmed that the small suspended cells remained small attached cells (see Fig. S1 and also Ref. 14), and so we used the optical images taken during AFM-indentation to quantify the attached cell size within unsorted populations, and assign that cell objectively as a large cell that would have been D^{hi} in the suspended state or a small cell that would have been D^{lo} in the suspended state.

Figure S5c shows that the distribution of the relative nuclear fluctuations of O1 and O4 cells are consistent with the relative nuclear fluctuation of unsorted, large cells (spread area > 5500 μm^2) and small cells (spread area < 5000 μm^2) before sorting. For these distributions, we again used optical images to objectively distinguish the larger and smaller cells in unsorted populations.

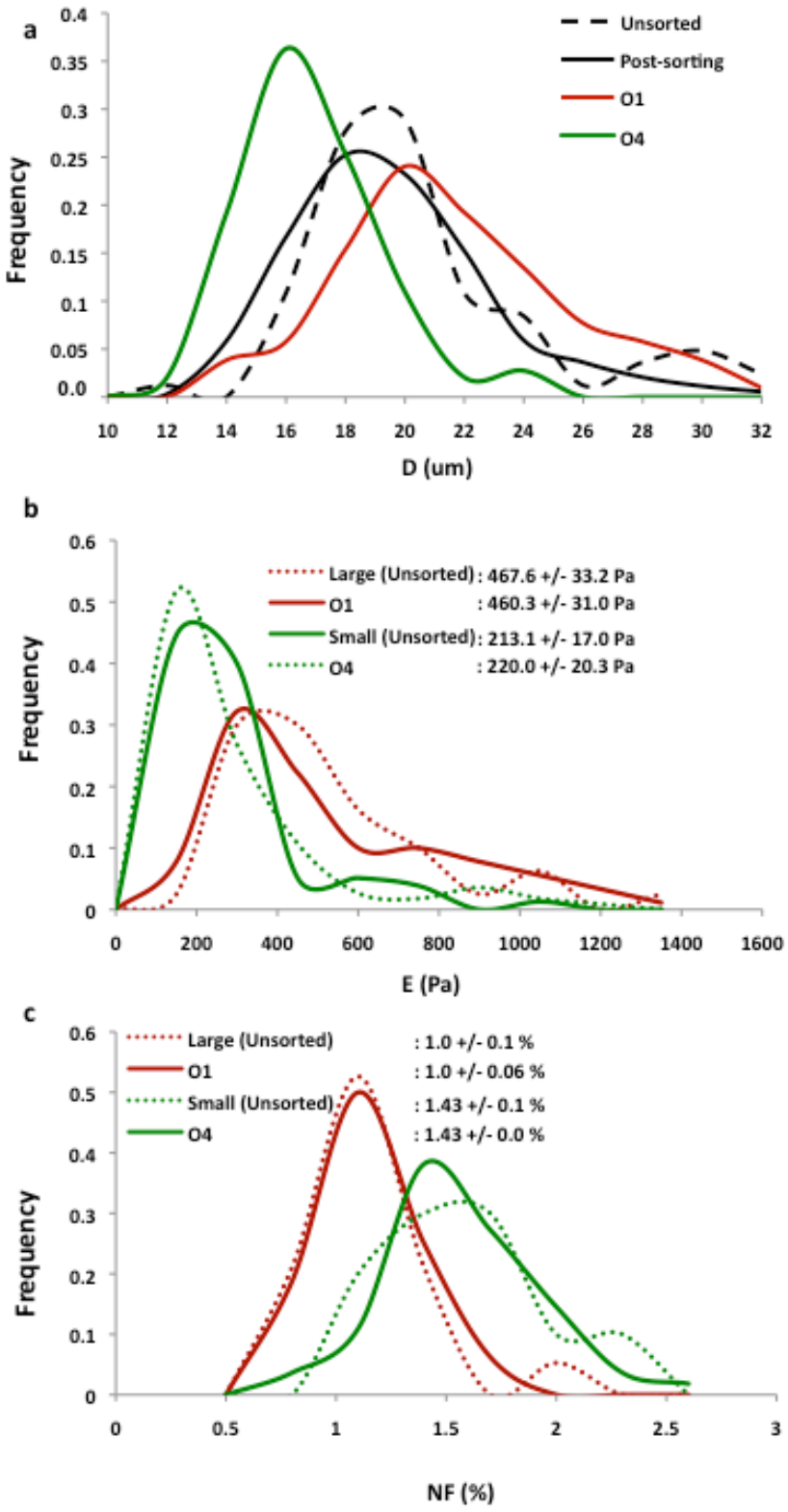

Figure S5. Spiral microfluidic sorting does not change the three biophysical properties of MSCs associated with multipotency. Distributions of biophysical properties for MSCs from donor aD3 in terms of (a) cell diameter *D*, before and after sorting; (b) cell stiffness *E*, for sorted D^{hi} (Outlet 1) and D^{lo} (Outlet 4) cells, as compared to large (cell spread area > 5500 μm^2) and small (spread area < 5000 μm^2) cells in the unsorted population; and (c) nuclear fluctuations *NF*, for sorted D^{hi} and D^{lo} subpopulations, as compared to large and small cells in the unsorted population.

4. Multivariate biophysical identification of multipotent MSC subpopulations.

Table 1 of the main text quantifies the magnitude of the three biophysical characteristics found to correlate with multipotent MSCs: cell diameter *D*, cell stiffness *E*, and nuclear fluctuations *NF*. **Figure S6** shows these data graphically, where each color represents a biophysically defined subpopulation for which *D*, *E*, or *NF* is categorized as relatively high or relatively low. This three-dimensional rendering makes clear that the multipotent subpopulation is a distinct group defined as $D^{lo}E^{lo}NF^{hi}$ (within the shaded box of Fig. S6), and the remaining groups are bipotent. This 3D rendering also shows that although some D^{lo} MSC subpopulations are bipotent (yellow, teal, and blue groups in Fig. S6), D^{hi} MSC subpopulations are all bipotent (osteochondral progenitor) subpopulations. See Table S3 for further discussion of Spearman correlations between each individual biophysical property and potency.

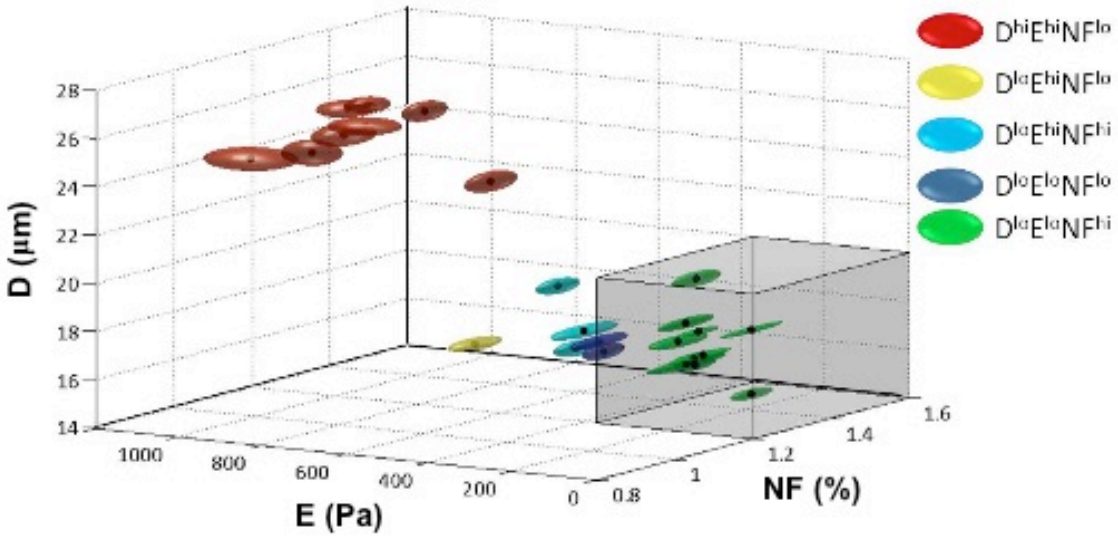

Figure S6. Graphical depiction of biophysical markers that correlated with MSC behavior *in vitro* and *in vivo*. Data correspond to that shown in Table 1, and are indicated as mean values (points) +/- SEM (ellipsoids) for each of the three biophysical characteristics of cell diameter *D*, cell stiffness *E*, and nuclear fluctuations *NF* (mean +/- SEM). Shaded box indicates parameter space corresponding to multipotent subpopulations (green), and remaining points in this three-dimensional parameter space correspond to bipotent, osteochondral progenitors.

These data could also be represented as bootstrapped distributions of means. In addition to the bootstrapped distributions of mean cell stiffness *E* shown in Figs. 2a-b of the main text, in **Figure S7** we also include those for mean cell diameter *D* and mean nuclear fluctuations *NF* for all MSC donor (sub)populations in Table 1. *NF* was also expressed as data points (mean +/- SEM) in Figs. 2c-d. Bipotent subpopulations are indicated in red while multipotent are indicated in green; no single one of these three biophysical parameters identifies multipotent subpopulations, which are $D^{lo}E^{lo}NF^{hi}$. Future work may consider the nature of these distributions among donor sources and may further refine the thresholds.

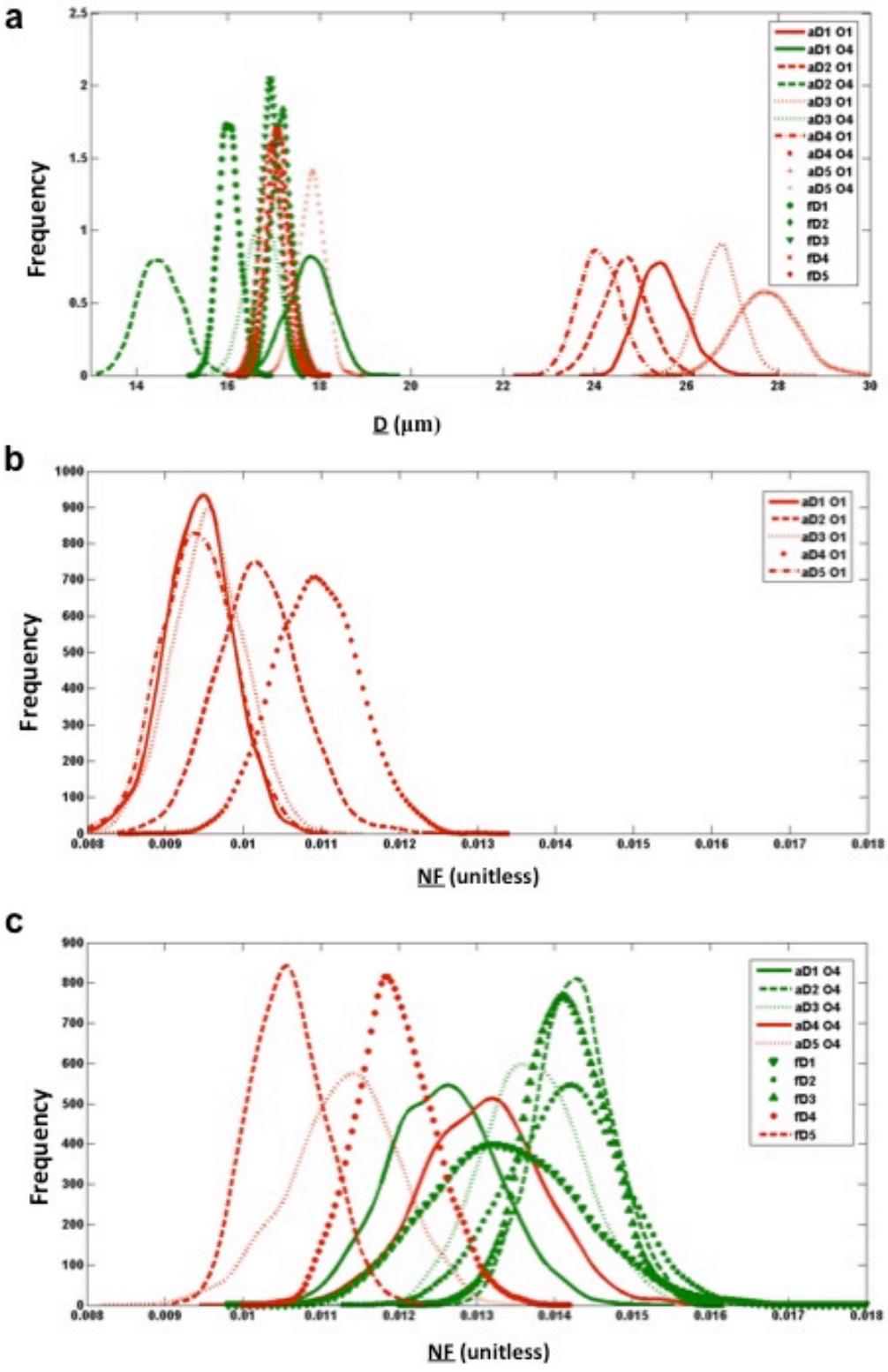

Figure S7. Distributions of mean (a) cell diameter *D* and (b, O1; c, O4) nuclear fluctuations *NF* for all MSC donor (sub)populations at passage 5. O1 and O4 are outlets 1 and 4, respectively, of the microfluidic device separating aMSCs by *D*. Red and green indicate bipotent and multipotent subpopulations, respectively. Distributions constructed via statistical bootstrapping, as described in

Methods for $\underline{E}$. As discussed in the manuscript, multipotent subpopulations were characterized by $\underline{D}$ > 20 μm or D^{hi}, $\underline{E}$ > 375 Pa or E^{hi}, and $\underline{NF}$ > 1.2% or NF^{hi}. See Fig. 2c, d for *NF* as mean +/- SEM.

5. Putative MSC surface markers do not distinguish biophysical subpopulations.

Figure S8 summarizes flow cytometry data for aMSCs, unsorted or sorted by cell size, and also fMSCs. All four groups demonstrated a consistent phenotype for the six, commonly used biomolecular markers considered: nonhematopoietic, nonendothelial, and positive for typical putative MSC markers, CD105 and CD90. Immunophenotyping against these biomolecular characteristics did not resolve differences among subpopulations that differed significantly in multivariate biophysical characteristics (e.g., as seen here by the similar profiles of unsorted, D^{hi} and D^{lo} subpopulations from aD1), and that differed significantly in differentiation potential (bipotent vs. multipotent).

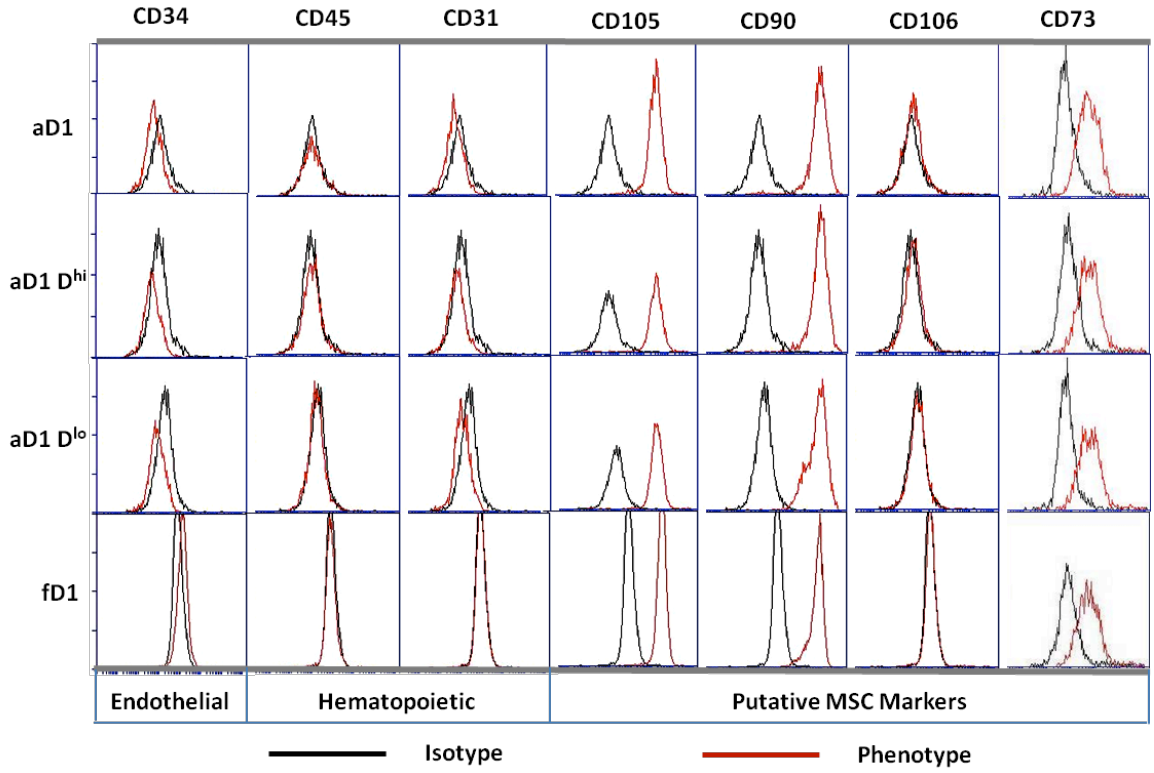

Figure S8. Immunophenotype of putative MSCs as obtained via flow cytometry of fluorescent antibody-labeled cells, shown as cell associated fluorescence vs. number of events, from representative donor sources aD1 and fD1 at passage 5. All groups show similar antigen surface profiles, despite measureable differences in biophysical properties and *in vitro* or *in vivo* characteristics.

6. Comparison of MSC biophysical properties and potency at passages 5 and 8.

Table S1 compares the three biophysical properties indicative of MSC multipotent subpopulations at passage 5 (P5) to those measured at passage 8 (P8). This table also indicates the potency at each of these passages, as either (osteochondral) bipotent or multipotent. Here, the notation of the cell population indicates the donor (e.g., aD1) and the inertial microfluidic outlet from which the subpopulation was collected (e.g., O1 for Outlet 1, which comprises the larger cells), if applicable. Figure S13 illustrates schematically that cells were expanded separately to passage 5 and to passage 8 from unsorted MSC populations, prior to biophysical and functional analysis.

More importantly, one observes that mean suspended-cell diameter $\underline{D}$ did not change appreciably between passages 5 and 8 for a given donor and subpopulation; this is of course expected, in that that aMSCs were physically sorted into outlets that separate on the basis of size, and in the fMSCs are noted not to change appreciably in morphology from passage to passage. One also observes that cell stiffness $\underline{E}$ and nuclear fluctuations $\underline{NF}$ did not necessarily change within measurement sensitivity, between passages 5 and 8 for a given donor. Most intradonor comparisons (e.g., P5 vs. P8 for aD1 O1) were within the standard error of measurement (SEM). More importantly, the overall category (e.g., $D^{lo}E^{lo}NF^{hi}$) for each subpopulation remained the same between passage 5 and 8; and the potency (bipotent or multipotent) remained the same between passage 5 and 8 for that MSC subpopulation. In other words, multiple biophysical markers (specifically cell diameter, cell stiffness, and nuclear fluctuations) predict differential potency of sorted subpopulations of MSCs, even when different passage numbers are considered.

When we compare this finding with the *unsorted* MSC populations of aD1-aD3 in **Table S2** at passages 5 and 8, we see that unsorted MSCs from a given donor can shift in potency. Note that in two of three donors expanded to P8, the fraction of O4 (smaller) MSCs decreased relative to that at P5, and that in these expansions the potency shifted from multipotency to bipotency. In the donor for which the unsorted population remained multipotent as defined in the text and Fig. 2 and Fig. S3, note that the relative decrease in the O4 cells was also lower. Specifically, unsorted MSCs from aD1 and aD2 were categorized as multipotent at P5, but as bipotent at P8. In contrast, unsorted MSCs from aD3 were multipotent at both passages.

This change in unsorted population-level biophysical properties and potency can be explained plausibly by either (1) shifts in the prevalence of cells comprising the bipotent subpopulations in aD1 and aD3; or (2) shifts in the overall biological and biophysical characteristics of the unsorted MSCs with increased passaging. Either scenario is possible, as MSCs are sensitive to culture condition changes that can occur upon repeated handling and passaging; and because it has been shown that larger MSCs can result from smaller MSCs that have exited the cell cycle (14). For aD1 and aD2, this shift in the unsorted MSC potency can be attributed most plausibly to an increase in the relative prevalence of D^{hi} MSCs (shown in the last column as the ratio of cells collected from Outlet 1 to those from Outlet 4, O1:O4). This is a ~five- to tenfold increase in Outlet 1 (D^{hi}) MSCs. Table S1 and Fig. S6 show that (Outlet 1) D^{hi} MSC subpopulations are stiffer and biopotent for aD1 and aD2, so the increased prevalence of cells within that larger, stiffer subpopulation at passage 8 is reflected in the relative stiffening and bipotency of the unsorted population at passage 8. aD3 shows only a

fourfold increase in the larger cell subpopulation at passage 8, relative to passage 5. Together, these comparisons suggest that a change in relative prevalence of the smaller cells (as required of multipotency) can signal a potential for change in the potency of the unsorted population.

In fact, such passage number-dependent or passage condition-dependent shifts underscore the importance of approaches that identify and devices that can biophysically sort MSCs at each passage: this provides means to distinguish and separate the bipotent and multipotent subpopulations.

Table S1. Biophysical markers from different subpopulations of MSCs, expressed as mean +/- SEM, for both passage 5 (approximately population doubling 10-12 for all sources) and passage 8 for selected sources. NA indicates subcultures that did not expand robustly to P8. Corresponding population potency is indicated in green (multipotent: adipo-, osteo-, chondro- and myogenic,) or red (bipotent: osteo-, chondrogenic), respectively. Mean *D*, *E*, and *NF* corresponding to values below (for *D* and *E*) and above (for *NF*) bipotency thresholds discussed in the text are indicated in green; and otherwise in red. See Fig. S13 for schematic, illustrating how cells were obtained at P5 and P8.

	Cell Pop.	Passage No.	D (μm)	E (Pa)	NF (%)	Category	Potency
aMSCs	aD1 O1	5	25.5 ± 0.5	813.85 ± 64.72	0.94 ± 0.04	$D^{hi}E^{hi}NF^{lo}$	Bipotent
		8	27.0 ± 0.3	804.41 ± 58.86	1.02 ± 0.05	$D^{hi}E^{hi}NF^{lo}$	Bipotent
	aD2 O1	5	24.6 ± 0.4	460.30 ± 31.00	1.02 ± 0.06	$D^{hi}E^{hi}NF^{lo}$	Bipotent
		8	26.2 ± 0.4	765.28 ± 56.52	0.97 ± 0.06	$D^{hi}E^{hi}NF^{lo}$	Bipotent
	aD3 O1	5	26.7 ± 0.3	705.69 ± 76.65	0.96 ± 0.05	$D^{hi}E^{hi}NF^{lo}$	Bipotent
		8	27.9 ± 0.3	653.59 ± 42.79	0.91 ± 0.04	$D^{hi}E^{hi}NF^{lo}$	Bipotent
	aD4 O1	5	24.1 ± 0.4	1100.31 ± 99.57	1.09 ± 0.06	$D^{hi}E^{hi}NF^{lo}$	Bipotent
		8			NA		
	aD5 O1	5	27.7 ± 0.4	543.84 ± 30.92	0.94 ± 0.05	$D^{hi}E^{hi}NF^{lo}$	Bipotent
		8			NA		
	aD1 O4	5	17.8 ± 0.2	274.88 ± 19.32	1.32 ± 0.07	$D^{lo}E^{lo}NF^{hi}$	Multipotent
		8	16.6 ± 0.1	223.85 ± 18.71	1.31 ± 0.07	$D^{lo}E^{lo}NF^{hi}$	Multipotent
	aD2 O4	5	14.5 ± 0.2	220.00 ± 20.29	1.43 ± 0.05	$D^{lo}E^{lo}NF^{hi}$	Multipotent
		8	15.9 ± 0.2	329. 68 ± 18.50	1.40 ± 0.06	$D^{lo}E^{lo}NF^{hi}$	Multipotent
	aD3 O4	5	16.7 ± 0.2	340.05 ±28.75	1.37 ± 0.07	$D^{lo}E^{lo}NF^{hi}$	Multipotent
		8	15.5 ± 0.2	345.84 ± 16.28	1.42 ± 0.05	$D^{lo}E^{lo}NF^{hi}$	Multipotent
	aD4 O4	5	17.1 ± 0.2	508.86 ± 33.02	1.31 ± 0.08	$D^{lo}E^{hi}NF^{hi}$	Bipotent
		8			NA		
	aD5 O4	5	17.8 ± 0.2	304.55 ± 25.34	1.13 ± 0.07	$D^{lo}E^{lo}NF^{lo}$	Bipotent
		8			NA		
fMSCs	fD1	5	16.0 ± 0.2	291.43 ± 18.63	1.34 ± 0.10	$D^{lo}E^{lo}NF^{hi}$	Multipotent
		8	19.2 ± 0.3	323.95 ± 20.50	1.40 ± 0.06	$D^{lo}E^{lo}NF^{hi}$	Multipotent
	fD2	5	17.2 ± 0.1	210.96 ± 14.00	1.42 ± 0.08	$D^{lo}E^{lo}NF^{hi}$	Multipotent
		8			NA		
	fD3	5	16.9 ± 0.1	338.32 ± 16.95	1.42 ± 0.05	$D^{lo}E^{lo}NF^{hi}$	Multipotent
		8			NA		
	fD4	5	17.0 ± 0.3	425.46 ± 26.33	1.20 ± 0.05	$D^{lo}E^{hi}NF^{hi}$	Bipotent
		8	17.4 ± 0.2	563.66 ± 33.78	1.09 ± 0.06	$D^{lo}E^{hi}NF^{lo}$	Bipotent
	fD5	5	17.1 ± 0.3	340.51 ± 22.36	1.18 ± 0.05	$D^{lo}E^{lo}NF^{lo}$	Bipotent
		8	19.5 ± 0.3	468.36 ± 24.69	1.20 ± 0.05	$D^{lo}E^{hi}NF^{hi}$	Bipotent

Table S2. Biophysical markers from different *unsorted* populations of aMSCs, expressed as mean +/- SEM, for both passage 5 (approximately population doubling 10-12 for all sources) and passage 8 for selected sources. Control indicates that these are unsorted MSC populations. [O1]:[O4] ratio represents the relative prevalence of Outlet 1 cells to Outlet 4 cells in the unsorted population. NA indicates subcultures that did not expand robustly to P8. See Fig. S13 for schematic, illustrating how cells were obtained at P5 and P8.

Cell Pop.	Passage No.	D (μm)	E (Pa)	NF (%)	Potency	[O1] : [O4]
aD1	5	23.6 ± 4.1	434.35 ± 32.53	1.19 ± 0.04	Multipotent	1.14
Control	8		639.17 ± 48.24	1.13 ± 0.04	Bipotent	10.80
aD2	5	21.2 ± 4.0	323.63 ± 25.44	1.13 ± 0.05	Multipotent	0.82
Control	8		493.44 ± 27.38	1.12 ± 0.03	Bipotent	3.64
aD3	5	21.4 ± 3.9	582.48 ± 54.50	1.23 ± 0.04	Multipotent	0.60
Control	8		495.75 ± 23.75	1.12 ± 0.04	Multipotent	2.50
aD4	5	24.1 ± 4.1	861.87 ± 77.32	1.24 ± 0.04	Bipotent	1.20
Control	8			NA		
aD5	5	23.6 ± 4.5	466.36 ± 23.21	1.05 ± 0.04	Bipotent	1.75
Control	8			NA		

7. Correlation between biophysical descriptors of MSC subpopulations and multipotency.

Table S3 summarizes the Spearman correlations used to analyze the strength of correlations between a given MSC subpopulation-level biophysical property and potency. Significant correlation was observed for *E*, *NF*, and *D*, as indicated by two-tailed p-values < 0.05, while correlations with *A* and *N:C* were not significant. Note that MSC subpopulations with larger diameter were also bipotent; those larger cells were also stiffer and of lower nuclear fluctuations than the other subpopulations. (See Fig. S6 for three-dimensional graph of biophysical markers that correlate with potency.) However, as discussed in the text, subpopulations of smaller diameter were not necessarily multipotent, and this is supported by the existent but weaker correlation of cell diameter with multipotency shown in Table S3. Multipotent subpopulations are correlated with small cell diameter, low mechanical stiffness, and low nuclear fluctuations, as demonstrated graphically in Fig. S6.

Table S3. Correlation between MSC biophysical properties and multilineage differentiation capacity for *E* (cell elastic modulus), *NF* (nuclear fluctuation), *D* (suspended cell diameter), *A* (cell spread area) and *N : C* (nuclear to cytoplasmic ratio).

Correlations	E (Pa)	NF (%)	D (μm)	A (μm^2)	N : C
Number of XY Pairs	15	15	15	15	15
Spearman r	-0.7874	0.8519	-0.5517	-0.1336	-0.2453
95% confidence interval	-0.9285 to -0.4478	0.5919 to 0.9514	-0.8347 to -0.03813	-0.6485 to 0.4651	-0.7108 to 0.3695
P value (two-tailed)	0.0005	< 0.0001	0.0330	0.6634	0.4192
Correlation level	Strong	Strong	Weak	No	No

Table S4 shows how much *D*, *E*, and *NF* differ between O1 and O4 for passage 5. On average, for a given donor the larger-cell subpopulation comprised cells that were 60% larger, 150% stiffer, and exhibited 25% lower nuclear fluctuations as compared to the smaller-cell subpopulation.

Table S4. Percentage by which cell diameter, stiffness and nuclear fluctuations differed for each aMSC donor source. This comparison is based on cells that were sorted by size into outlet 1 (O1) of the inertial micfofluidic device, as compared to O4.

Donor	Passage No.	D (μm)	E (Pa)	NF (%)
aD1	5	+ 43.3%	+ 196.1%	- 28.8%
	8	+ 62.7%	+ 259.4%	- 22.3%
aD2	5	+ 69.7%	+ 109.2%	- 28.7%
	8	+ 64.8%	+ 132.1%	- 30.7%
aD3	5	+ 59.9%	+ 107.5%	- 29.9%
	8	+ 80.0%	+ 190.0%	- 35.9%
aD4	5	+ 40.9%	+ 116.2%	- 16.8%
	8		NA	
aD5	5	+ 55.6%	+ 78.6%	-16.8%
	8		NA	
Average		+ 60.6%	+ 148.6%	-26.2%

8. Effects of cell divisions on biophysical properties of MSC subpopulations

Although the focus of this manuscript is multivariate biophysical analysis of MSC multipotency for a given donor and cell passage number, one may ask whether these properties change upon cell division. Specifically, does cell division promote biophysical heterogeneity? It is important to keep in mind that in the present work we quantified and compared biophysical properties of the subpopulation, not individual cells, and we did not attempt to synchronize the cell cycles within the unsorted or sorted populations.

In summary, over long timescales of many passages or population doublings, the biophysical properties of a subpopulation remain fixed but the prevalence of that subpopulation changes (Tables S1-S2). This long timescale is also discussed in SI Section 6. Over intermediate timescales of several population doublings but a single passage, the cell size changes cyclically upon cell division; if one or both of the cell daughters exits the cell cycle, the cell size will increase (14). However, for one or fewer full population doublings, we did not detect a difference in D or E or NF of cells within a given subpopulation. This finding relates back to the observations at long timescales, indicating shifts in subpopulation prevalence for MSCs over extended passages. Of relevance to the current focus on biophysical descriptors of MSC multipotency, it is important to note that $D^{lo}E^{lo}NF^{hi}$ appears to describe the multipotent subpopulation, regardless of when or why or how the prevalence of that subpopulation changes.

First, Table S1 of the paper compares the biophysical properties of cell subpopulations from a given donor source at passage 5 and at passage 8. This corresponds to about six population doublings between the two analyses, or a relatively long timescale. Importantly, all nine of these comparisons show that the subpopulation potency (bipotent or multipotent) is unaffected by passaging from P5 to P8. One can observe the "Category" of each subpopulation (e.g., the $D^{hi}E^{hi}NF^{lo}$ triplet for aD1 O1 at passage 5), and ask whether this category changes after those in vitro population doublings (e.g., still $D^{hi}E^{hi}NF^{lo}$ for aD1 O1 at passage 8). Considering all nine comparisons that can be made from these data in Table S1 (P5 vs. P8 for a given donor and/or outlet), we note that 8 of the 9 comparisons show no change in the biophysical descriptor of the subpopulation (as in the above example for aD1 O1, which remains described as $D^{hi}E^{hi}NF^{lo}$). In the one case where the biophysical triplet changes between P5 and P8, this is for fMSC fD5, and the difference is only in whether the mean cell stiffness $\underline{E}$ is considered high or low according to the thresholds in the text ($\underline{E}$ > 375 Pa for E^{hi}). Given that the $\underline{E}$ here is just below the threshold for passage 5, there are several reasons that could explain this shift, related to the data distributions or potential unnoted changes in culture conditions between passages. Again, however, the potency of a subpopulation was unaffected by passaging from P5 to P8.

Second, Table S2 shows that the unsorted or "control" MSC populations from adult donors do change in apparent potency. This point is already noted in discussion of Table S2. Both aD1 and aD2 unsorted MSCs were characterized as multipotent at passage 5, and then as only bipotent at passage 8. Table S1 shows that the biophysical triplets of the Outlet 1 and Outlet 4 subpopulations remained the same for these donors, so what explains this shift in potency of

the unsorted MSCs? Here, note in Table S2 the relative prevalence of the Outlet 1 (larger) cells has increased considerably. There are more of the larger, bipotent cells at passage 8, so as a heterogeneous unsorted population it reflects a bipotent response in the suite of *in vitro* differentiation assays used. In other words, the biophysical properties of a subpopulation can remain fixed, but the number of cells within that subpopulation can change with passaging (or, just as possible, with a change in one or more culture conditions).

Third, it is reasonable to next ask what causes such changes in prevalence of the smaller and larger cells within the unsorted MSC population. Some of us considered this previously in Ref. 14, via timelapse image analysis and tracking of cell divisions over one week (a single passage). Briefly, those experiments and simulations showed that a "small MSC" becomes a "large MSC" when the cell exits the cell cycle. In that paper, Whitfield et al. also showed that (as well-known) the cell area increases upon cell division and then decreases when two daughter cells are generated, so the cell size does change continuously and cyclically upon cell division. Whitfield et al. further illustrated the well-known stochastic nature of that division: not all cells were actively dividing over a "population doubling." For cells that exceed that "mitotic division" maximum, though, the cell stops dividing, increases in cell volume and area, but remains adherent within the culture. These observations showed that the larger cells are not necessarily a stable subpopulation that continues to actively divide, nor "old" cells, but rather cells that have exited the cell cycle (as would be expected in the pathway toward phenotypic commitment). Thus, a mother cell can be different in size from its daughter cells, but only slightly so if both the mother and the daughters continue to self-replicate. If D^{lo} cells exit the cell cycle, they will "get bigger" and perhaps be individually described as D^{hi} cells.

Fourth, for the data shown in this paper, we did naturally consider such timescales of <1 full population doubling because we measured *E* and *NF* up to 48 hours after division (i.e., less than and approaching one full population doubling). For example, for aD3 O4 at P5, we found no marked difference in cell size ($\underline{D}$ = 16.7 ± 0.2 μm at 24 h, vs. 17.1 ± 0.3 μm at 48 h post-sorting; and found no marked difference in stiffness ($\underline{E}$ = 329.68 ± 18.5Pa at 24 h, vs. 337.37 ± 19.3Pa at 48 h post-seeding) or nuclear fluctuations ($\underline{NF}$ = 1.4 ± 0.06%, with a data range of 0.9% < *NF* < 2% that indicated no trend over 36 h) for aD2 O4 at P8. That is, whether we measured these properties at less than one population doubling (< 24 h), or approximately one population doubling (~36-48 h), there was no detectable shift. We also confirmed that cells that were D^{lo} in the suspended state remained small cells in the adherent state, up to 48 hrs post-seeding (Fig. S1).

Finally, taken together these data show that $D^{lo}E^{lo}NF^{hi}$ appears to describe the multipotent subpopulation even when prevalence of that subpopulation changes.

9. Rationale for analysis of subpopulations, rather than colonies

We demonstrated that multipotent subpopulations of bone marrow-derived MSCs also form more colonies and proliferate more rapidly (Fig. 3). These hallmarks of self-renewal are

considered characteristic of stem cells, but biological assays of MSCs can often also include clonal analyses. One may anticipate that this approach could more rigorously define "stemness" if one were to prove that all cells within a given biophysically defined subpopulation (e.g., $D^{lo}E^{lo}NF^{hi}$ that are multipotent) were demonstrated to produce colonies with progeny that exhibited the same characteristics (i.e., all such colonies comprised cells that were $D^{lo}E^{lo}NF^{hi}$). In other words, why did we not also show a single-cell or clonal correlation between these properties and function? Although such clonal assays may be considered an important topic of future studies, there are several reasons why we did not and cannot take that approach in this study.

First, our primary stated motivation in identifying these biophysical characteristics is for identifying multipotent or progenitor cells in culture-expanded populations. This is because the clinical community recognizes an outstanding challenge in identifying donor sources and culture-expanded cell populations of predictable properties – for those clinical applications, the number of cells required is too large to expand from a single cell. Practically, it is of high relevance to understand how subpopulations within the culture expansions comprising millions of cells can be distinguished. Our approach and findings support that goal of ultimately sorting MSC subpopulations in large numbers and with predictable *in vitro* or *in vivo* outcome. This "subpopulation" charactetrization approach is also similar in spirit to how flow cytometry is used to separate subpopulations based on surface antigens.

Second, one cannot straightforwardly probe these cell biophysical properties and then the differentiation potential of that cell or of a clonal population, without potentially introducing many additional complexities. Specifically, several papers have noted (or shown in raw data without noting explicitly in the text) that even clonal populations have the capacity for physical or functional heterogeneity upon expansion. For example, Mets et al. noted that smaller cells gave rise to larger cells in cloning experiments (8); DiGirolomo et al. noted considerable variation in extent of differentiation, "even in comparisons of large colonies isolated from the same plate from the same donor" (9); Colter et al. noted that colonies derived from single cells contained both "spindle-shaped and large flat cells (1); and Bianco et al. (10) referred to sork of Sacchetti et al.(11) when noting that stochastic commitment or senescence in culture even among clonal progeny is as yet undefined. Anecdotally, Ylostalo et al. noted that signle-cell colonies were heterogeneous, with cells in the inner regions differing from those in the outer with respect to both morphology and commitment (12); and Neuhuber et al. noted without much detail that some flat cells were observed in colonies expanded from a signel small MSC, and some small cells were observed in populations "expanded from a flat MSC founder" (13). Cells within or derived from a single clone can then come to differ in biophysical or functional properties. We have also recently demonstrated that progeny from a *single* mesenchymal stromal cell can, over as short an *in vitro* duration as one week, change significantly in size and associated markers of lineage commitment (14). This actually underscores the relevance of our subpopulation-based approach: regardless of why or when heterogeneity ensues in culture-expanded MSCs, these biophysical markers can be used to identify cell subpoulations within that mixture that are either multipotent or bipotent progenitors.

Third, and more specific to the biophysical experiments in this study, here we used inertial microfluidics in order to separate the initially heterogeneous MSC population into groups defined in part by suspended cell diameter *D*. This sorting device is based on inertial flow and requires relatively high cell concentrations and fluid volumes to operate on this principle efficiently. That requirement matched well with our practical goal of working with large culture-expanded populations, after which we could conduct additional assays of stiffness, nuclear fluctuations, and other characteristics of the "small" and "large" subpopulations. That requirement would not be met by using a colony defined as a few to tens of progeny; further expansion introduces the potential for emergent heterogeneities as discussed above.

B. Detailed Methods, including Supporting Figures S9-S13

Samples, animals and ethics. Cells analyzed herein were derived from bone marrow of five adult and five fetal donors, each obtained from commercial or consortia sources of low-passage, putative MSCs (adult donors) or from established centrifugation and plastic-adherence subculture methods (fetal donors (15)). These cell populations from each donor source were thus considered to be mesenchymal stem cells according to existing, accepted methods. All fetal human tissue collection for research purposes was approved by the Domain Specific Review Board of the National University Hospital in Singapore, in compliance with international guidelines for the use of fetal tissue in research (16). In all cases, donors gave separate written consent for the use of the collected fetal tissue Fetal femurs were collected for isolation of fMSCs after clinically indicated termination of pregnancy. Samples correspond to 10-14 weeks gestation (N = 5). Human adult MSC samples used in this study were obtained from commercial sources (N = 5). Non-obese diabetic/severe combined immunodeficient (NOD/SCID) mice were acquired through Charles Rivers, Australia, and all in vivo procedures were approved by the Institutional Animal Care and Use Committee at the National University of Singapore.

Cell culture. Human adult bone marrow derived MSCs were obtained as passage 2 from donors in a random sampling of single-donor commercial sources (Lonza, ReachBio) and the US NIH National Center for Research Resources-funded Tulane University of Health Sciences Center. Human fetal bone marrow derived MSCs were isolated as previously described (15, 17). Briefly, single-cell suspension were prepared using a 22-gauge needle, passing through a 70-μm cell strainer (BD Biosciences) and plating on culture flasks (Nunc) in DMEM at 10^6 cells/ml. Adherent spindle-shaped cells were recovered from primary culture 4-7 days later. Non-adherent cells were removed with initial medium changes every 2-3 days. At subconfluence, they were trypsinized and replated at an initial low density (10^4 cells/cm^2). For both adult and fetal cell donor sources, experiments were performed across multiple passages with passaging cell seeding density of 500 cells/cm^2. Results presented in the main text correspond to passage 5 among all samples for consistency; supporting information provides corresponding data for select populations at multiple passages. Routine culture for all MSCs was conducted in Dulbecco's modified Eagle's medium (DMEM)-Glutamax (Gibco) supplemented with batch selected 10% fetal bovine serum (FBS), 50U/ml penicillin,and streptomycin (Gibco) in a humidified 37°C, 5% CO_2.

Statistical analysis. All data are presented as mean ± SEM unless otherwise noted. For quantitative analysis of MSC *in vitro* (N = 3) and *in vivo* differentiation (N = 5) and quantitative RT-PCR, biological replicates from each subpopulation were analysed and the statistical significance of the differences was estimated using two-tailed, unpaired student's *t*-tests ($\alpha = 0.05$). To construct histograms of cell stiffness distributions, statistical bootstrapping including resampling with replacement was conducted as outlined by Efron (18) and described more fully in analysis of *E*, with the resampled data set comprising the 30-60 replicate experiments (i.e., cells) per subpopulation and condition, and resamplings to obtain

convergent mean and standard error of *E* as shown in Fig. 2, Table 1 and Table S1. To investigate correlations between mechanical properties and multipotency, Spearman correlation coefficients (r) were calculated and expressed as r ± 95% confidence intervals using Prism (GraphPad) software, with two-tailed p values <0.01 indicating strong correlation, <0.05 indicating weak but existent correlation, and >0.1 indicating insignificant correlation.

BIOPHYSICAL CHARACTERIZATION.

Size-based cell sorting: MSCs were sorted as a function of suspended-cell diameter *D* using a spiral microchannel device that has been described previously for other applications (19). The microchannel design consisted of 9-loop spiral geometry with single inlet and eight bifurcating outlets. Briefly, MSCs were expanded at a low seeding density of 500 cells/cm^2 on tissue culture polystyrene and incubated for 5 days so that they were approximately 50% confluent before they were trypsinized and sorted. Cells were resuspended in culture media at a density of 50-100k cells/mL and introduced into the microchannel via a syringe pump at an optimized flow rate of 1.5 mL/min. aMSCs exhibiting an initially broad size distribution were separated into distinct trajectories at different lateral positions along the microchannel cross-section under the influence of inertial lift and Dean drag forces. By the time the flow streams reached the outlets, the cells were efficiently separated into four fractions of distinct diameter distributions at Outlets 1 (largest), 2, 3 and 4 (smallest), respectively. Cells from Outlets 1 and 4 were then collected for subsequent analysis. Cell diameter *D* was quantified post-sorting via optical image analysis (Image J, NIH). See Supporting Information and Fig. S1 for further discussion.

Cell stiffness, or indentation elastic modulus: MSCs harvested from sorting or subculture were seeded on sterilized 24 mm-diameter coverslips and maintained overnight in 36 mm-diameter Petri dishes in the incubator prior to indentation. During indentation, cells were maintained in CO_2 independent medium (Invitrogen) at 37^{o}C using the BioCell (JPK instruments, Germany) on a NanoWizard II atomic force microscope (AFM; JPK Instruments, Germany) coupled with an inverted optical microscope (Olympus, Japan).

A modified silicon nitride AFM cantilever (NovaScan, USA) with a spring constant of 0.03 N/m with a 4.5 μm-diameter polystyrene bead adhered to the cantilever free end was used to indent the cells. Indentation was carried out at the center of the cell body (see **Fig. S9**; this central region typically sampled over the nucleus), under a piezoactuated displacement rate of 1 μm/s. A maximum indentation force ranging from 200 pN to 400 pN was applied in order to ensure that a small deformation was exerted on the cell (typically depths of 50-400 nm and nominal strains of 15%) and minimized mechanical contributions from the underlying stiff polystyrene coverslip. The effective Young's elastic modulus *E* of each cell was subsequently determined using the modified Hertzian contact model implemented within JPK data processing software (JPK Instruments, Germany), and at least 30 individual cells were sampled for each population and experimental condition.

For figure display, the values of *E* generated from each subpopulation (30-60 individual cells per condition, with multiple indentation locations per cell body center) were then analyzed via statistical bootstrapping (18) to visualize mean and standard error, as described previously (20). Briefly, from a measured set of *E* values from *n* different cells, a new set of *n* values was obtained by resampling with replacement. The mean of this new set was then calculated, and the sampling process was repeated until the standard deviation of these bootstrapped means suitabley converged, which occurred within 2000 iterations. This standard deviation, multiplied by a factor approaximately equal to 1 ($\sqrt{n/(n-1)}$), serves as an estimate for the standard error of the mean. In each case, the average mean of the bootstrapped sets matched the mean of the original set, indicating negligible estimator bias. The resulting distributions of bootstrapped means were graphed in Matlab (The Mathworks). This statistical bootstrapping process was also used to generate Fig. S7 for cell diameter and nuclear fluctuation data.

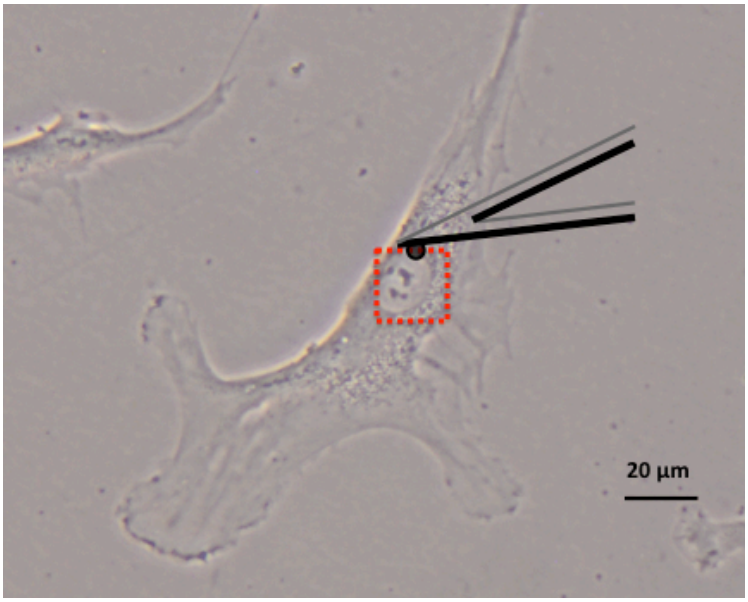

Figure S9. Schematic illustrating relative scale and position of spherical, cantilevered probe of 4.5 µm diameter used to acquire atomic force microscopy-enabled nanoindenation data to depths of 50-400 nm at the center of the cell body (multiple indentations spaced within red square), from which the effective Young's elastic modulus *E* of the cell was computed.

Nuclear membrane fluctuations: MSCs harvested from sorting or subcultures were seeded on sterile glass-bottom Petri dishes, maintained in the incubator overnight before transfection. Cells were transfected with 500ng of pEGFP-LaminB1 C1 plasmid (G. Shivshankar) using Lipofectamine 2000 and Opti-MEM (Invitrogen). Cells were imaged 24 h later via timelapse optical microscopy (LSM 780 confocal microscope; Carl Zeiss, Germany). Briefly, images (512×512 pixels) at a single, fixed focal plane (corresponding to the maximum nucleus perimeter) were captured with optimal pinhole aperture size for a duration of ~7.5 min over 5 sec intervals (i.e., 90 frames) for each cell using C-Apochromat 63×/1.4 NA water immersion objective. For each cell population and experimental condition, 30 to 50 cells were imaged

and analyzed. Images were converted to binary images after noise reduction using Image-J, and then analyzed by a Matlab (The Mathworks) program using a genetic algorithm. Details regarding the calculation of average relative nuclear fluctuations are provided in **Fig. S10**.

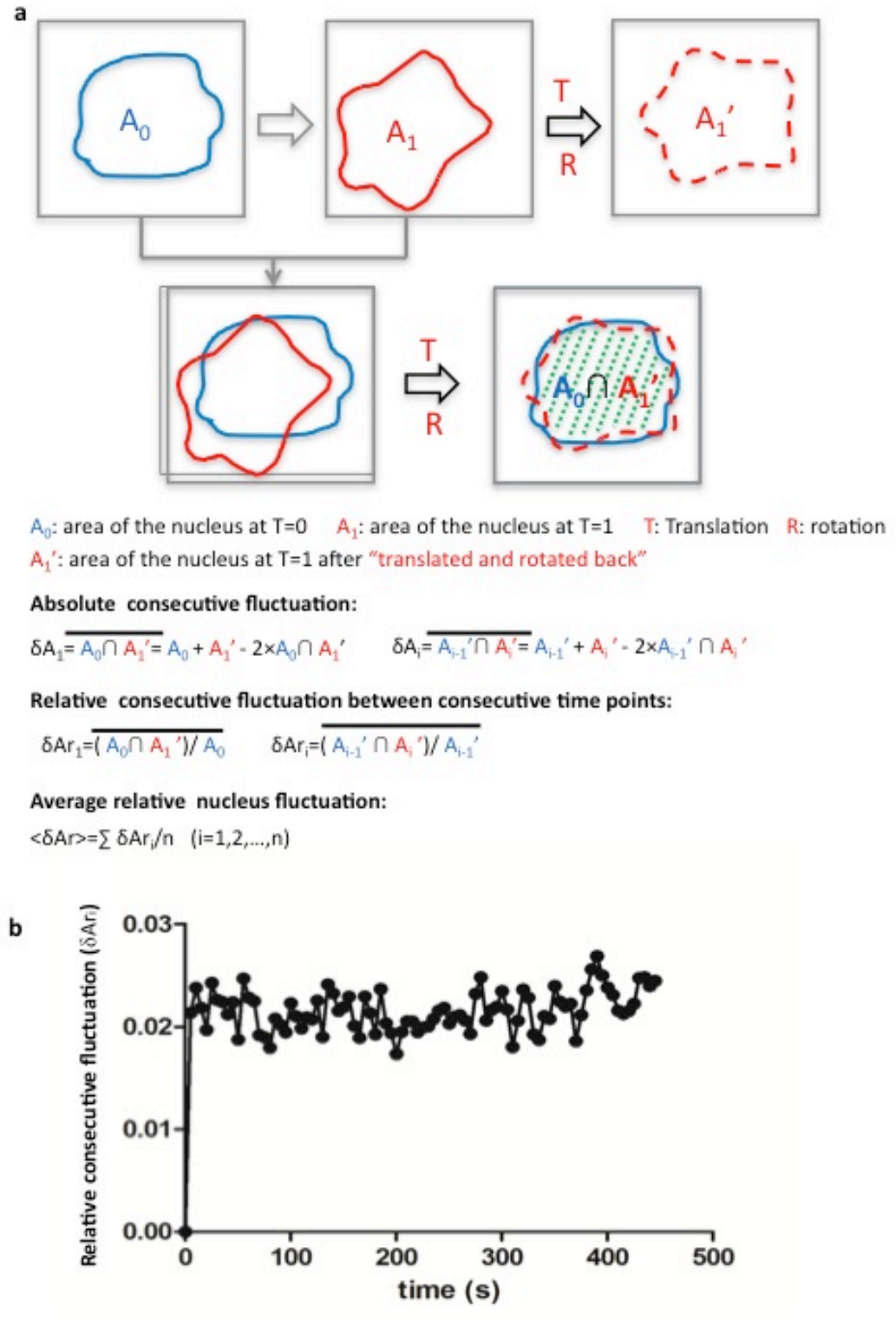

Figure S10. (a) Schematic illustrating calculation of relative nuclear fluctuation (<δAr>)**.** (b) Typical time series of relative consecutive nuclear fluctuation (δAr_i).

Cell spread area and nucleus-to-cytoplasm volumetric ratio: Cells seeded on glass-based Petri dishes were 4% PFA fixed, 0.01% Triton permeablized, and then stained with Heochest and Rhodamine Phalloidin (Invitrogen). Tiled confocal (3D) images were captured with the optimal pinhole aperture size using a LSM 780 confocal microscope (Carl Zeiss, Germany) with C-Apochromat 63×/1.4 NA water immersion objective. The images were then analyzed using Imaris (Bitplane AG) to obtain the cell spread area and the nucleus to cytoplasm volumetric ratio.

Colony formation assays: Colony formation unit (CFU-F) efficiency assays were conducted for the biophysically distinct groups, and for unsorted aMSCs. Cells from each group were seeded at 4 cells/cm^2 in 100mm dishes (200 cells per dish) in basal media under standard subculture conditions described above, and the percentage of CFUs counted at day 14 via optical microscopy by staining with Crystal Violet. Representative data are shown in Fig. 3q of the manuscript, and **Figure S11a** below shows these data for all MSC donor groups considered. Note that multipotent subpopulations showed higher CFU-F efficiency than biopotent MSC subpopulations.

Cell proliferation assays: Cell proliferation rates were assessed by seeding cells in basal complete media as described above for subculture, and monitoring the number of cells per unit area over 18 days. Cells from each group were seeded at 500 cells/cm^2 in basal media under standard subculture conditions described above, and counted via hemocytometry at each timepoint. Representative data from each biophysically distinct group are shown in Fig. 3r of the manuscript, and **Figure S11b** below shows these data for all MSC donor groups considered. Note that multipotent subpopulations (green) exhibited higher proliferation rates than bipotent MSC populations (red).

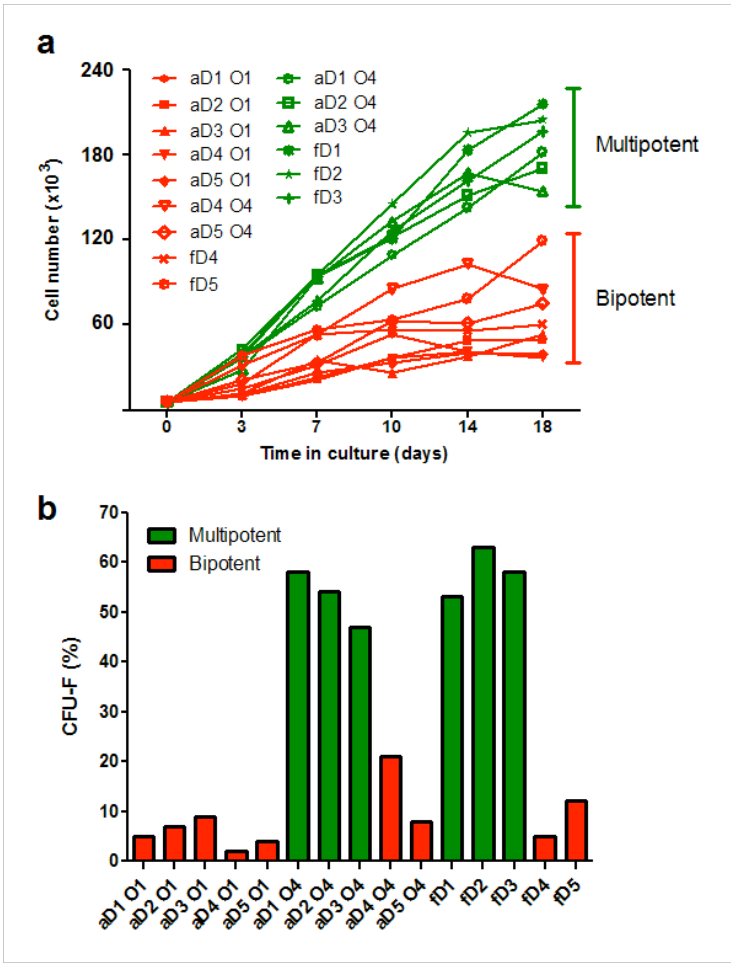

Figure S11. Additional in vitro quantification of MSC colony formation and proliferation at passage 5. (a) Cell number as a function of days in culture for all MSC donor (sub)populations. (b) Colony forming units (CFU-F) for all MSC donor (sub)populations, assayed via staining at day 14. Red and green indicate bipotent and multipotent subpopulations, as indicated in Table 1.

BIOCHEMICAL CHARACTERIZATION.

Immunophenotyping and immunofluorescence. MSCs were trypsinized and washed in phosphate buffered saline (PBS). Non-specific antigens were blocked by incubating the cells in PBS containing 1% bovine serum albumin (BSA) for 1 h at 37°C. For immunophenotyping, cells were screened for CD14, CD34, CD45, CD31, and CD105 (SH2) (all purchased from R&D Systems) by fluorescent activated cell sorter (FACS) as described previously(21). For immunofluorescence, cells were permeabilized in 0.1% Triton X-100 in PBS, blocked with 1% BSA. Primary antibody labeling for osteopontin (Santa Cruz) and desmin (Abcam) was performed in 1% BSA in PBS for 8-16 h at 4°C. Secondary antibody labeling was performed using the same procedure with Alexa-488-labeled goat anti-mouse IgG containing rhodamine-phalloidin and DAPI (Invitrogen). Early osteogenic differentiation was detected using alkaline phosphatase staining (Vector Labs) by incubating the cells in the substrate solution for 30 min before visualization at 594 nm excitation wavelength via optical microscopy (epifluorescence). Immunofluorescence microscopy was conducted using an

Olympus IX81 epi-fluorescent microscope. Images were exported into ImageJ (NIH) for analysis.

In vitro **multilineage differentiation and quantitative analysis.** For adipogenic induction, MSCs were plated at 2 X 10^4 cells/cm^2 and cultured in adipogenic differentiation medium (DMEM supplemented with 5μg/ml insulin, 10^{-6} dexamethasone, and 0.6 X 10^{-4} indomethacin) for up to 3 weeks, with medium exchanges three times per week. To visually detect cytoplasmic lipid accumulation, cultures were fixed in 4% paraformaldehyde for 20 min and stained with 0.3% Oil Red O (Sigma-Aldrich) in 0.6% isopropanol for 1 h. The content of Oil Red O in samples were quantified by extraction with 100% isopropanol for 5 min followed by spectrophotometry quantification at 510 nm(22). For osteogenic induction, MSCs were plated at 2 X 10^4 and cultured in osteogenic differentiation medium (DMEM supplemented with 10mM β-glycerophosphate, 10^{-8} M dexamethasone, and 0.2mM ascorbic acid) for up to 14 days, with medium changes three times per week. Extracellular accumulation of calcium was assessed by Alizarin Red S staining. The stained monolayer was extracted with 10% acetic acid (v/v) and neutralized with 10% (v/v) ammonium hydroxide followed by colorimetric quantification at 405nm(23). The alkaline phosphatase activity in cell lysates was measured using SensoLyte pNPP Alkaline Phosphatase Assay Kit (AnaSpec) and normalized to total cell number. Briefly, suspended cells were lysed in 0.1% of Triton-X, centrifuged at 2500g for 10 min for 4ºC. Fifty (50) μL of the supernatant was incubated with 50 μL of the pNPP substrate solution for 30 min before the absorbance of the mixture was measured at 405 nm. For chondrogenic differentiation, MSCs were pelleted and cultured in chondrogenic differentiation medium (DMEM supplemented with 0.1 μM dexamethasone, 0.17 mM ascorbic acid, 1.0 mM sodium pyruvate, 0.35 mM L-proline, 1% insulin-transferrin sodium-selenite (Themo Fischer Scientific, Singapore), 1.25 mg/ml bovine serum albumin, 5.33 μg/ml linoleic acid, and 0.01 μg/ml transforming growth factor-β) for 28 days with medium changed three times per week. The micromass pellets were formalin fixed, paraffin embedded, and sectioned in 10 μm slices. Thereafter, they were dewaxed and rehydrated before Alcian Blue (Sigma-Aldrich) staining. Cells were then rinsed three times with distilled water and the amount of cell-associated dye was measured at 620 nm, after extraction with 6 M guanidine-HCl (Sigma-Aldrich) (24). For myogenic induction, MSCs were plated at 3000 cells/cm^2 and cultured in myogenic induction medium (DMEM supplemented with 3μM 5'Azacytidine) for 24 h before the induction medium was replaced with basal DMEM for up to 3 weeks with medium changes three times per week. Myogenic differentiation was analyzed by immunostaining the differentiated cells and counting the number of cells immunopositive for desmin.

RNA isolation and microarray. RNA samples were prepared with Qiagen RNEasy Kits and quality checked with an Agilent Bioanalyzer chip before analysis (RIN = 9 - 10, both 260/230 and 260/280 are above 1.8). Microarray hybridization was conducted by a service core facility at the Agency for Science, Research and Technology (A*STAR) Singapore. The

HT-12 chip (Illumina), which is capable of assaying >48,000 human transcripts, was used for this analysis. All reagents and equipment used for hybridization were purchased from Illumina. Statistical analysis of microarray data comparign the four biophysical groups defined by *D*, *E*, and *NF* was performed by an independent researcher (A*STAR Singapore).

Semiquantitative RT-PCR. All RNA samples were prepared using Qiagen RNEasy Kits. RTPCR analysis was performed using the Express one step SYBR green kits (Invitrogen) on a StepOnePlus system (Agilent). Primer sequences of osteogenic genes were as follows (5' to 3'): runx2 (NM_001024630.3) (F: CGAATGGCAGCACGCTATTA, R: TGGCTTCCATCAGCGTCAA), osteopontin (NM_000582.2) (F: CGGGACCAGACTCGTCTCA, R: TTCCTTGGTCGGCGTTTG), osteocalcin (NM_199173.4) (F: TCCACAGCCTTTGTGTCCAA, R: GCGCCTGGGTCTCTTCACTA), gapdh (F: CAAGGCTGTGGGCAAGGT, R: GGAAGGCCATGCCAGTGA). RTPCR was performed in triplicate and thermal cycle conditions were 50^{o}C for 2 min, 95^{o}C for 10 min, then 50 cycles at 95^{o} for 15 sec and 60^{o}C for 1 min. Amplifications were monitored with the ABI Prism 7000 Sequece Detection System (Applied Biosystems). Results were normalized against the housekeeping gene glyceraldehyde-3-phosphate dehydrogenase (GADPH), and relative gene expression was analyzed with the 2^{-ddCt} method.

IN VIVO **ANALYSIS.**

Scaffold loading and *in vivo* transplantation for ectopic bone assays. Polycaprolactone-tricalcium phosphate (PCL-TCP) 3D bioactive scaffolds (Osteopore International) with a lay-down pattern of 0/60/120^{o}, porosity of 70% and average pore size of 0.523 mm were used in 5X5X5 mm dimensions. The scaffolds were treated with 5M NaOH for 3 h to enhance hydrophilicity and washed thoroughly with PBS thrice prior to ethanol sterilization. Each cell-seeded scaffold included a cell subpopulation (or unsorted cells, as indicated) from only a single donor source; subpopulations of shared biophysical characteristics but different donor sources were not pooled. MSCs were suspended in Tisseel Fibrin Sealant (Baxter) before seeding into the porous scaffolds (2 x 10^5 cells per scaffold); acellular scaffolds served as cell-free controls. Scaffolds were then conditioned in osteogenic differentiation medium for 1 week before implantation. Before implantation, a midline longitudinal skin incision was made on the dorsal surface of each NOD-SCID mouse under general anaesthesia by inhalation of isofluorane/O_2. Subcutaneous pockets were created and the MSC cellular scaffold constructs were inserted. The skin was then closed with 5-O Vicryl sutures. To determine the degree of osteogenesis in these scaffold, we injected a bisphosphonate agent every week (OsteoSense 750, Perkin Elmer) at the recommended dosage. OsteoSense is a hydroxyapatite-specific dye that accumulates in sites of active bone modeling. To determine the degree of osteogenesis in these scaffold, we injected a bisphosphonate agent (OsteoSense 750, Perkin Elmer) every week over 4 weeks at a concentration of 2 nmol/100 µL at 100µL per mouse. Mice were sacrificed 24 h after the last injection and the scaffolds were removed

surgically for analysis via fluorescence imaging with a Xenogen IVIS system (EX: 745 nm, EM: 800 nm). The cumulative fluorescent signal from each scaffold was quantified with ROI tools.

Muscle regeneration *in vivo*. NOD-SCID mice were anaesthetized and 15 µg of cardiotoxin (Molecular Probes) was injected into the gastrocnemius muscle 3 h prior to cell transplantation. Mice were then re-anaesthetized, and MSCs suspended in 35 µl saline were slowly injected into the injured muscles. Each cell injection comprised a cell subpopulation (or unsorted cells, as indicated) from only a single donor source; subpopulations of shared biophysical characteristics but different donor sources were not pooled. Mice were sacrificed 3 weeks later and the muscle was harvested, fixed in 1.5% PFA, mounted in embedding medium (Sakura) and sectioned as 10 µm thick transverse sections on glass slides. The sections were washed in PBS three times before immunostaining with human specific beta-2-microglobulin, muscle specific spectrin and DAPI. Stained sections were examined under LSM 780 confocal microscope (Carl Zeiss).

Figure 5a-c in the manuscript summarizes the total radiant efficiency of th ectopic bone mineralization for representative MSC donor sources from each biophysically distinct group (e.g., $D^{lo}E^{lo}NF^{hi}$). **Figure S12a** provides these data for all MSC donor groups. Note that subpopulations categorized as bipotent in Table 1 exhibited high radiant efficiency as compared to those categorized as multipotent ($D^{lo}E^{lo}NF^{hi}$). Figure 5d in the manuscript compares spectrin formation at injured muscles injected with biophysically distinct groups of MSCs. **Figure S12b** also provides these images for all MSC donor groups. Note that all subpopulations categorized as multipotent in Table 1 exhibited evidene of myogenic differentiation via staining for human spectrin, wheraas bipotent subpopulations did not.

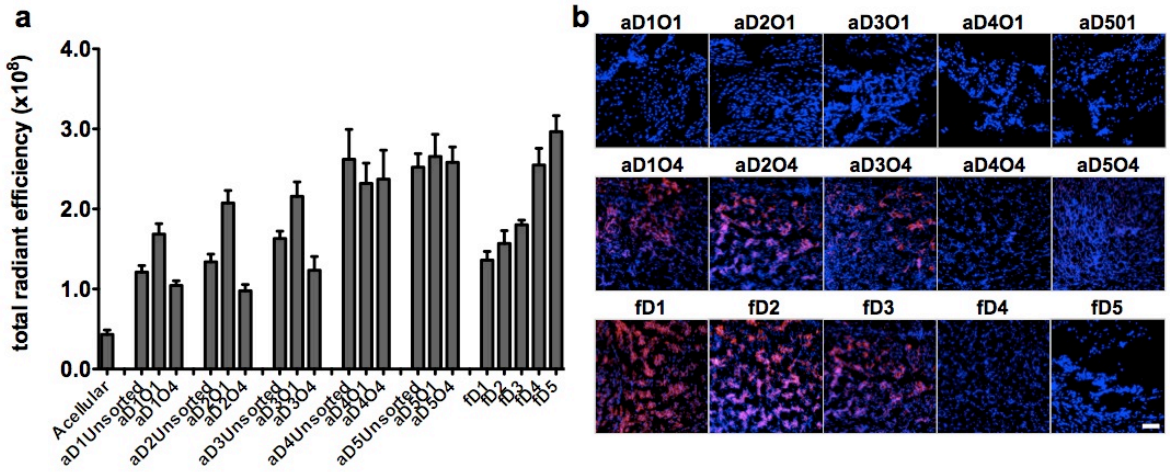

Figure S12. Additional data for in vivo assays. (a) Total radiant efficiency (Osteosense) for ectopic bone mineralization assays, corresponding to each MSC donor group. Figure 5 includes a representative subset of these data. (b) Histological sections of spectrin formation (red) within injured skeletal muscle tissue injected. Cell nuclei stained with Hoechst (blue), and human spectrin with labeled antibody (magenta). Figure 5 includes a representative subset of these images. Scalebar, 100 µm.

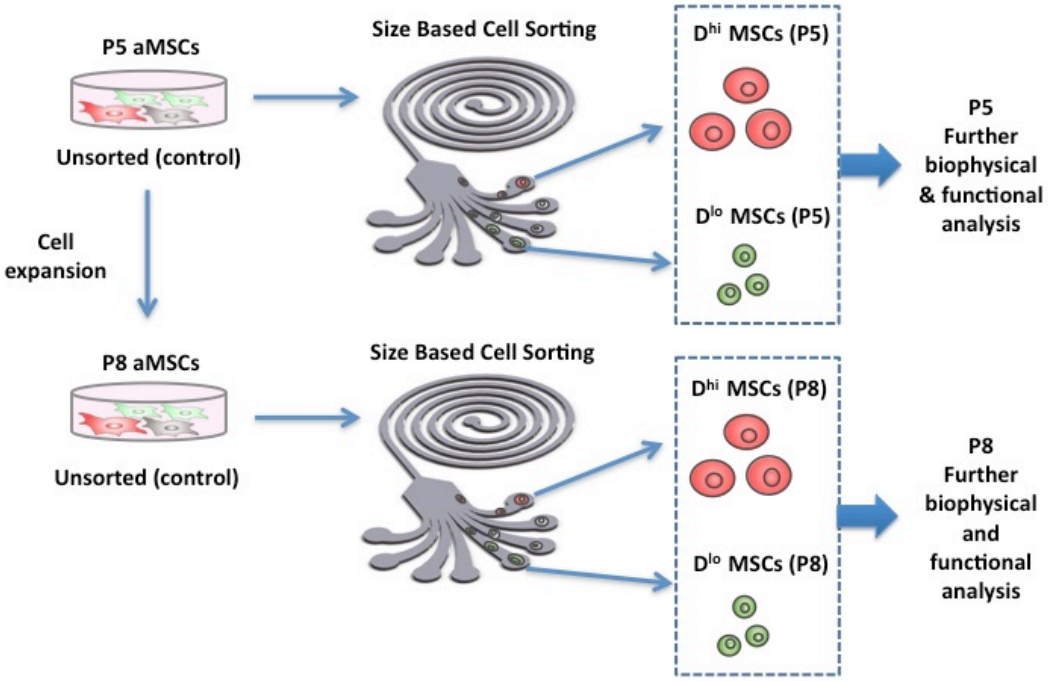

Figure S13. Schematic illustrating comparisons at two different passage numbers, summarized in Tables S1 and S2. Results reported for cells at passage 5 were obtained by sorting cells at passage 5 (P5) via the microfluidic device, and characterized in terms of biophysical properties and in vitro or in vivo functional properties for an unsorted (control) population, as well as cell subpopulations from outlet 1 (O1, D^{hi}) and outlet 4 (O4, D^{lo}) of the device. The unsorted P5 cells were also expanded to passage 8 (P8), and that expanded culture from unsorted MSCs was used to obtain an unsorted (control) populations as well as cell subpopulations from outlets 1 (D^{hi}) and 4 (D^{lo}) for P8.

C. References

1. Colter DC, Sekiya I, & Prockop DJ (2001) Identification of a subpopulation of rapidly self-renewing and multipotential adult stem cells in colonies of human marrow stromal cells. *Proc Natl Acad Sci U S A* 98(14):7841-7845.

2. Guillot PV, Gotherstrom C, Chan J, Kurata H, & Fisk NM (2007) Human first-trimester fetal MSC express pluripotency markers and grow faster and have longer telomeres than adult MSC. *Stem Cells* 25(3):646-654.

3. Jo CH*, et al.* (2008) Fetal mesenchymal stem cells derived from human umbilical cord sustain primitive characteristics during extensive expansion. *Cell and Tissue Research* 334(3):423-433.

4. Gonzalez-Cruz RD, Fonseca VC, & Darling EM (Cellular mechanical properties reflect the differentiation potential of adipose-derived mesenchymal stem cells. *Proc Natl Acad Sci U S A* 109(24):E1523-1529.

5. Chowdhury F*, et al.* (Material properties of the cell dictate stress-induced spreading and differentiation in embryonic stem cells. *Nat Mater* 9(1):82-88.

6. Bhattacharya D, Talwar S, Mazumder A, & Shivashankar GV (2009) Spatio-temporal plasticity in chromatin organization in mouse cell differentiation and during Drosophila embryogenesis. *Biophys J* 96(9):3832-3839.

7. Oh SK*, et al.* (2005) Derivation and characterization of new human embryonic stem cell lines: SNUhES1, SNUhES2, and SNUhES3. *Stem Cells* 23(2):211-219.

8. Mets T & Verdonk G (1981) In vitro aging of human bone marrow derived stromal cells. *Mech Ageing Dev* 16(1):81-89.

9. Digirolamo CM*, et al.* (1999) Propagation and senescence of human marrow stromal cells in culture: a simple colony-forming assay identifies samples with the greatest potential to propagate and differentiate. *Br J Haematol* 107(2):275-281.

10. Bianco P, Robey PG, & Simmons PJ (2008) Mesenchymal stem cells: revisiting history, concepts, and assays. *Cell Stem Cell* 2(4):313-319.

11. Sacchetti B*, et al.* (2007) Self-renewing osteoprogenitors in bone marrow sinusoids can organize a hematopoietic microenvironment. *Cell* 131(2):324-336.

12. Ylostalo J, Bazhanov N, & Prockop DJ (2008) Reversible commitment to differentiation by human multipotent stromal cells in single-cell-derived colonies. *Exp Hematol* 36(10):1390-1402.

13. Neuhuber B, Swanger SA, Howard L, Mackay A, & Fischer I (2008) Effects of plating density and culture time on bone marrow stromal cell characteristics. *Exp Hematol* 36(9):1176-1185.

14. Whitfield MJ, Lee WC, & Van Vliet KJ (Onset of heterogeneity in culture-expanded bone marrow stromal cells. *Stem Cell Res* 11(3):1365-1377.

15. Chan J*, et al.* (2005) Human fetal mesenchymal stem cells as vehicles for gene delivery. *Stem Cells* 23(1):93-102.

16. Polkinghorne J (1989) Review of the Guidance on the Research Use of Fetuses and Fetal Material. *CM 762. London: HMSO*.

17. Chan J*, et al.* (2007) Widespread distribution and muscle differentiation of human fetal mesenchymal cells after intrauterine transplantation in dystrophic mdx mouse. *Stem Cells* 25(4):875-884.

18. Efron B (1979) 1977 Rietz Lecture - Bootstrap Methods - Another Look at the Jackknife. *Annals of Statistics* 7(1):1-26.

19. Kwon OS*, et al.* (2008) Photoaging-associated changes in epidermal proliferative cell fractions in vivo. *Arch Dermatol Res* 300(1):47-52.

20. Maloney JM*, et al.* Mesenchymal stem cell mechanics from the attached to the suspended state. *Biophys J* 99(8):2479-2487.

21. Campagnoli C*, et al.* (2001) Identification of mesenchymal stem/progenitor cells in human first-trimester fetal blood, liver, and bone marrow. *Blood* 98(8):2396-2402.

22. Sekiya I*, et al.* (2002) Expansion of human adult stem cells from bone marrow stroma: conditions that maximize the yields of early progenitors and evaluate their quality. *Stem Cells* 20(6):530-541.

23. Gregory CA, Gunn WG, Peister A, & Prockop DJ (2004) An Alizarin red-based assay of mineralization by adherent cells in culture: comparison with cetylpyridinium chloride extraction. *Analytical Biochemistry* 329(1):77-84.

24. Nishigaki F*, et al.* (2002) FK506 induces chondrogenic differentiation of clonal mouse embryonic carcinoma cells, ATDC5. *European Journal of Pharmacology* 437(3):123-128.